Dalton Transactions

ROYAL SOCIETY OF CHEMISTRY

PAPER

View Article Online
View Journal | View Issue

Check for updates

Cite this: *Dalton Trans.*, 2024, **53**, 5521

Cyclotribenzylene alkynylgold(I) phosphine complexes: synthesis, chirality, and exchange of phosphine†

Jing Zhang,[a] Nathalie Zorn,[b] Emmanuelle Leize-Wagner,*[b] Marion Jean,[c] Nicolas Vanthuyne,*[c] Enrique Espinosa,[d] Emmanuel Aubert,*[d] Bruno Vincent[a] and Jean-Claude Chambron*[a]

Received 20th December 2023,
Accepted 22nd February 2024

DOI: 10.1039/d3dt04279k

rsc.li/dalton

Two different alkynyl-substituted C_3-symmetric cyclotribenzylenes (CTB) were synthesized in racemic and enantiomerically pure forms, and six gold(I) phosphine complexes differing by the nature of the CTB and the phosphine were prepared and characterized, in particular by NMR spectroscopy, DOSY, electronic circular dichroism (ECD), and electrospray ionization mass spectrometry (ESI-MS). Their ECD patterns depended on the substitution of the starting CTBs and were shifted bathochromically by comparison with the latter. ESI-MS in the presence of HCO_2H allowed us to detect the complexes as proton adducts. The intensities of the signals were stronger when the phosphine was more electron-rich. This technique was also used to investigate the exchange of phosphine betweeen pairs of CTB complexes. The scrambling reaction was demonstrated by the higher intensity of the signals of the complexes subjected to the exchange of a single phosphine ligand by comparison with the intensity of the signals of the starting complexes.

Introduction

Self-assembly under thermodynamic control is an efficient and expeditious tool for the synthesis of highly symmetrical cage-like molecular structures from simple components.[1] As a matter of fact, it has been used extensively for the construction of molecular containers and nanoreactors.[2,3] This synthetic approach takes advantage of bonding interactions that are reversible in certain conditions, such as hydrogen bonding,[4] coordination bonds,[5] dynamic covalent bonds,[6,7] and hydrophobic interactions.[8] Among other reversible but less common interactions, the Au(I)···Au(I) aurophilic bonding interaction is worth mentioning because it has an energy similar to that of a standard hydrogen bond.[9] This attractive interaction can occur, in the absence of steric hindrance, between linearly two-coordinate Au^+ ions at distances between 2.50 and 3.50 Å, that is, below the sum of their van der Waals radii (>4 Å).[10] The occurrence of aurophilic interactions in gold complexes stems from the low coordination geometry of Au(I) and the maximum relativistic contraction of gold orbitals. Therefore, among the identified M···M contacts, those involving Au(I) are the strongest. Aurophilic interactions have been identified, in particular, by single crystal X-ray crystallography analysis of several aryl acetylide gold(I) phosphine complexes, whether they were unsupported[11–15] or supported by covalent bonds,[16–19] and the so-called topological bonds.[20]

We have been interested for several years in the self-assembly and study of chiral metallacages based on tritopic cyclotribenzylene (CTB) organic ligands and $[ML]^{2+}$ assembling metal complex fragments (M = Pd, Pt; L = phosphine or diphosphine).[21,22] The first members of this family of compounds were reported in 2001 by Shinkai and coworkers.[23] Further developments in the last few decades were performed by the group of Hardie.[24–28] The structure, the stereochemistry, and the properties of CTB-based metallacages make them coordination complex analogues of the cryptophanes.[29–32] These latter compounds, which were designed four decades ago by Collet and coworkers, are macropolycyclic receptors. They feature a cavity lined by aromatic walls, and are able to host a great variety of substrates. The prototypical members of this family of compounds were shown to strongly complex hydro(halo)carbons, quaternary ammoniums, and the xenon atom. More recently, functionalized cryptophanes were used

[a]*Institut de Chimie de Strasbourg, UMR 7177 CNRS, Université de Strasbourg, 4, rue Blaise Pascal, F-67070 Strasbourg, France. E-mail: jcchambron@unistra.fr*
[b]*Chimie de la Matière Complexe, UMR 7140 CNRS, Université de Strasbourg, 4, rue Blaise Pascal, F-67070 Strasbourg, France*
[c]*Aix-Marseille Univ., CNRS, Centrale Marseille, iSm2, Marseille, France*
[d]*Université de Lorraine, CNRS, CRM2, F-54000 Nancy, France*

†Electronic supplementary information (ESI) available: Copies of NMR, ESI-MS, electronic absorption, and ECD (experimental and calculated) spectra; views of the calculated structures, ESI-MS spectra of the CTB mixtures, and the corresponding graphs. Tables of all spectroscopic data. See DOI: https://doi.org/10.1039/d3dt04279k

for the encapsulation of soft metal cations in aqueous solutions.[33,34] An organometallic cryptophane, obtained by external grafting of $[Cp^*Ru]^+$ complex fragments onto the CTB subunits of an organic cryptophane was shown to host lipophilic anions such as BF_4^-, PF_6^-, and $CF_3SO_3^-$.[35]

In a previous study, we reported on the preparation of a C_3-symmetric CTB bearing three ethynyl functions.[36] This compound was used as a precursor for the synthesis of three trinuclear CTB-based acetylide gold(I) phosphine complexes differing by the nature of the terminal phosphine (PPh_3, PCy_3, and PEt_3), which showed interesting luminescence properties. In $CHCl_3$ solution, the complexes exhibited a long-lived blue phosphorescence and a weak fluorescence in the UV. In addition, in MeOH-rich solvent mixtures, their UV emission switched to a green emission. As we observed the aggregation phenomenon concomitantly, we qualified this new emission as an aggregation induced emission (AIE). In this paper, we shall examine the consequences of a systematic variation of the nature of the phosphine and of the CTB on the solution and gas-phase structure of the complexes, their electronic and chiroptical properties, and their intermolecular interactions in the gas phase. In particular, the possibility of the alkynylgold (I) CTBs to form metallocryptophanes in solution by dimerization templated by Au···Au bonding will be scrutinized.

Results and discussion

Preparation and spectroscopic characterization

The chemical structures of the six alkynylgold(I) phosphine complexes **C1–C6** of this study and their cyclotribenzylene (CTB) precursors are shown in Fig. 1. The complexes derive from the ethynyl γ′-substituted cyclotribenzylenes CTB(H,C_2H)[36] and CTB(OMe,C_2H),[37] both displaying the C_3 symmetry, and the latter differing from the former by the methoxy substituents in γ position. Two groups of complexes were therefore synthesized and investigated, depending on the precursor CTB: **C1**, **C2**, and **C3** derive from CTB(H,C_2H), and **C4**, **C5**, and **C6** derive from CTB(OMe,C_2H). In each group, the complexes differed by the terminal phosphine ligand, with systematic variation of the balance between the steric congestion and the electrodonor character: PPh_3 for **C1** and **C4**, PPh_2Me for **C2** and **C5**, and $PPhMe_2$ for **C3** and **C6**.

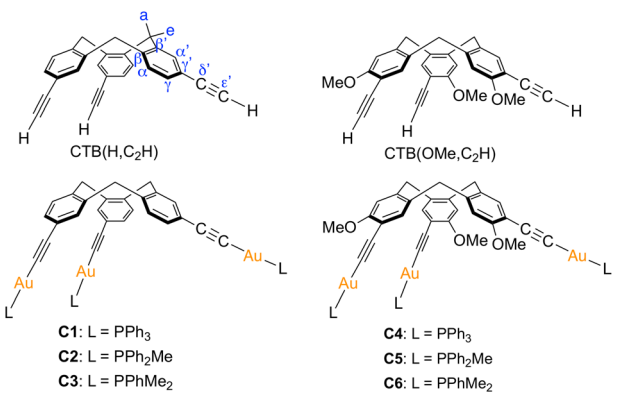

Fig. 1 Chemical structures of the CTBs (ligand precursors and complexes).

The complexes were prepared using either of the following methods of the literature: the first (method A) consists in the nucleophilic substitution reaction of the $[AuCl(PPh_nMe_{3-n})]$ complex by CTB(H,C_2H) or CTB(OMe,C_2H) in the presence of sodium methoxide and requires gentle heating,[38,39] whereas the second (method B) involves the cleavage of the presynthesized organometallic coordination polymer $[CTB(R,C_2Au)]_n$ (R = H or OMe) by a stoichiometric amount of the PPh_nMe_{3-n} phosphine at room temperature.[40,41] The yields were moderate to good (Table S1†). Method B showed higher simplicity than method A; it operates in milder conditions, and the product can be isolated without recrystallization.

The alkynylgold(I) CTB complexes were characterized by ^{1}H, ^{13}C, and ^{31}P NMR spectroscopies (Fig. S4–S33†), ESI-TOF mass spectrometry, IR spectroscopy, and elemental analysis. 1D NMR acquisitions were completed by 2D ^{1}H/^{1}H ROESY, ^{13}C/^{1}H HSQC, and ^{13}C/^{1}H HMBC experiments in order to assign the ^{1}H and the ^{13}C NMR spectra. The resulting NMR data including the complexation induced shifts (CIS) are collected in Tables S2 (^{1}H and ^{31}P) and S3 (^{13}C).†

Upon metallation of CTB(H,C_2H) and CTB(OMe,C_2H), the singlet of the alkynyl proton, at 3.02 and 3.24 ppm respectively, disappeared, providing a convenient method for monitoring the reaction by ^{1}H NMR spectroscopy. The typical CTB patterns were observed in the ^{1}H NMR spectra of the ligand precursors and correspond to molecules of C_3 symmetry: two pairs of doublets for the diastereotopic axial (a) and equatorial (e) protons of the methylene bridges; a doublet for each of the α and α′ protons and a doublet of doublets for the γ protons of CTB(H,C_2H); a singlet for each of the α and α′ protons of CTB(OMe,C_2H). The same patterns were observed in the ^{1}H NMR spectra of the corresponding gold complexes, which, in addition, showed the signals of the phosphine ligands. Noticeably, the signals of *o*-H (*o*′-H), which are the most deshielded of the aromatic protons, shifted downfield by +0.1 ppm increments upon going from **C1** to **C2** and **C3**, as a result of the stepwise replacement of a phenyl by a methyl substituent. A similar observation could be done within the series **C4**, **C5**, **C6**. Characteristic features of the methyl-substituted phosphine ligands were the doublets at *ca.* 2.05 ppm for PPh_2Me and *ca.* 1.75 ppm for $PPhMe_2$ with $^2J_{HP}$ ranging between 9 and 11 Hz. Doublets were also observed for the carbon atoms of the same methyl substituents at *ca.* 14.2 ppm for PPh_2Me and *ca.* 15.7 ppm for $PPhMe_2$ with $^1J_{PC}$ of *ca.* 35 Hz, and for the signals of the *ipso* (i-C), *ortho* (*o* and *o*′-C), and *para* (*p*-C) carbon atoms of the phenyl substituents with heteronuclear coupling constants of $^1J_{CP}$ = 55.3 Hz, $^2J_{CP}$ = 13.8, and $^3J_{CP}$ = 11.3 Hz (these values precisely for **C2**), respectively. The chemical shift of the phosphorus atom of the phosphine terminal ligand was independent of the CTB but depended on the nature of the phosphine: 43.0 ppm for PPh_3, 27.2 ppm for PPh_2Me, and 14.2 ppm for $PPhMe_2$. With regard to the ^{13}C

NMR spectra the signatures of the two series differed because of the presence of the methoxy substituent, which significantly impacted the chemical shifts of γ′-C (by *ca.* −11 ppm), α-C (by *ca.* −18 ppm), and γ-C (by *ca.* 28 ppm).

An interesting issue is the complexation-induced shifts ($\Delta\delta$ = CIS, see Tables S2 and S3†). In the case of **C1**, the protons α′-H were deshielded by +0.026 ppm, but α-H, γ-H, a-H and e-H were shielded by values ranging from −0.042 (γ-H) to −0.088 ppm (e-H) by comparison with CTB(H,C_2H). In the series **C1–C3** the CIS of α′-H and γ-H (protons *ortho* to the alkynyl substituents) were the most affected upon going from **C1** to **C2**, but showed only small changes when comparing **C2** and **C3**, indicating that the replacement of the first phenyl substituent by a methyl substituent had the strongest effect. In the case of the ^{13}C NMR spectra, only did the signals of the carbon atoms proximal to the metal, that is γ′-C, δ′-C and ε′-C, showed changes, moving downfield by +2.3 and +21 ppm, respectively. Comparison of the CTBs of the series **C4–C6** to their homologues of the series **C1–C3** showed that the chemical shifts of the CTB protons in **C4–C6** were less affected by metallation and by the nature of the phosphine co-ligand, α′-H excepted, the CIS of which decreased from +0.060 in **C4** to +0.036 in **C6**. The observations pertaining to the ^{13}C NMR spectra of complexes **C1–C3** hold true in the case of **C4–C6** as well.

The IR spectra of the complexes all showed the characteristic very weak (vw) absorption at *ca.* 2100 cm^{-1} corresponding to the ethynyl triple bond stretch. An absorption of medium (m) intensity at 1265 cm^{-1} was visible only in the spectra of the complexes **C4–C6**, which indicates that it corresponds to the C–O bond stretch of the arylether. Medium to strong (s) absorptions that were shared by all the spectra were found at *ca.* 1490 (m), 1435 (s), 1385 (weak for **C1**, but strong or medium for the others), 1100 (s or m), 735–745 (s or m), and 688–693 cm^{-1} (s or m).

Investigations of the nuclearities of the gold complexes

ESI-MS experiments. The alkynylgold(I) CTBs **C1–C6** were examined by electrospray ionisation mass spectrometry (ESI-MS) in the positive mode. The spectra are reproduced in Fig. S34–S45.† Before injection, 10^{-4} mol L^{-1} solutions in CH_2Cl_2 were diluted twice in i-PrOH/HCO_2H 1%, affording a final concentration of 5×10^{-5} mol L^{-1}. We found it necessary to run the experiments in acidic solutions despite the fact that the gold-alkynyl bond is acid-sensitive, because otherwise the molecular signal could be hardly detected. As a matter of fact, the main species that were identified are, in decreasing order of signal intensity: $[Au(PPh_nMe_{(3-n)})_2]^+$ > $[M\text{-}Au(PPh_n)Me_{(3-n)} + 2H]^+$ > $[M + H]^+$ > $[2M + 2H]^{2+}$, M corresponding to the complex **C*n***. We measured the ratio between the intensities of the signal of the species of interest and $[Au(PPh_nMe_{(3-n)})_2]^+$, the major ion that results from demetallation/reprotonation of the complexes in acidic conditions, as a function of E_{coll} (the energy, expressed in eV, used for collision-induced fragmentation) and plotted them for each complex (Fig. 2). Comparison of the graphs within each series **C1–C3** and **C4–C6** shows that

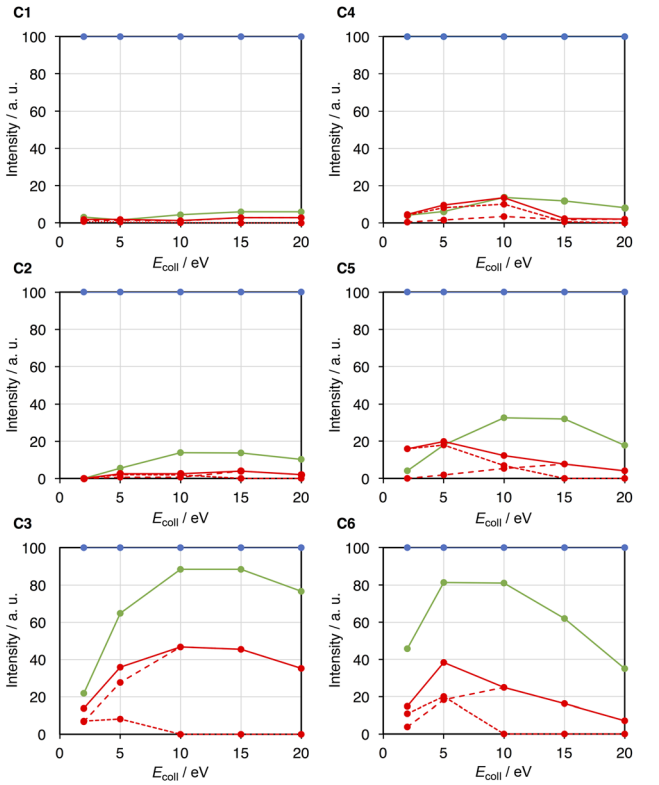

Fig. 2 Evolution of the intensities of the ESI-MS signals of the following ions: $[Au(PPh_nMe_{(3-n)})_2]^+$ (blue), $[M\text{-}Au(PPh_n)Me_{(3-n)} + 2H]^+$ (green), $[M + H]^+$ (red dashes) $[2M + 2H]^{2+}$ (red dots). The sum of the signals of $[M + H]^+$ and $[2M + 2H]^{2+}$ is represented by the red lines.

the more electron-rich the phosphine, the highest the intensities of the signals of the $[M\text{-}Au(PPh_n)Me_{(3-n)} + 2H]^+$ fragment and the molecular species (expressed as the sum of the signals of $[M + H]^+$ and $[2M + 2H]^{2+}$). Comparisons between **C1**/**C4** and **C2**/**C5** indicate that the substitution of OMe for H also increases the intensities of the signals of these two species, which is consistent with the concomitant increase of the electron richness of the CTB. In the case of **C3**/**C6** the differences are levelled out, as the intensities are higher for **C3** by comparison with **C6**. As the intensities of the molecular signal ($[M + H]^+$) and the signal of the fragment $[M\text{-}Au(PPh_n)Me_{(3-n)} + 2H]^+$ increase with the electron richness of the phosphine and CTB ligands, the observed trend reflects more the overall proton affinities than the stabilities of the complexes.

The plots in Fig. 2 also show the separate evolutions of the intensities of the signals of the doubly charged species associated with the molecular signal, $[2M + 2H]^{2+}$ (see also Table S4†). The intensity of the signal of $[2M + 2H]^{2+}$ is usually maximal at E_{coll} = 5 eV, excepted in the case of **C4**, for which it is maximal at E_{coll} = 10 eV. At the maximum, it increases in the order **C1** < **C2** < **C3** < **C4** < **C5** ≤ **C6**. Noticeably, experiments at higher concentration (10^{-3} mol L^{-1}) gave similar monomer to dimer ratios as those measured for **C2** (E_{coll} = 5 and 10 eV), **C5** (E_{coll} = 5, 10, and 20 eV), and **C6** (E_{coll} = 2 and 5 eV).

Table 1 DOSY data of CTB(H,C_2H) and the complexes **C1**, **C3**, and **C4**

Compound	Concentration ($\times 10^{-3}$ mol L^{-1})	T/K	Imaginary or real dimer: Dimensions[a] a/Å L/Å	b/Å d/Å	Ellipsoid v_m/Å^3 $4/3(\pi ab^2)$	Cylinder v_m/Å^3 $2\pi ab^2$	Solvent D_t [b]	Compound hydrodynamics: D_t [b]	r_H/Å[c]	v_H/Å^3 [d]	v_H/v_m
CTB(H,C_2H)[e]	—	298	5.31	6.69	995	—	30.30	8.64	6.17	980	0.98
C1	0.9	298	5.781	15.088	5510	—	16.50	4.23	10.40	4650	0.84
			13.910	30.176	—	9948		4.23	10.60	4980	0.50
	10	298	5.781	15.088	5510	—	16.90	3.89	11.10	5760	1.05
			13.910	30.176	—	9948		3.89	11.40	6180	0.62
C3	0.2	298	5.816	12.868	4030	—	23.80	5.01	9.16	3220	0.80
			11.632	25.736	—	6051		5.01	9.18	3240	0.54
	10	298	5.816	12.868	4030	—	20.60	4.82	9.46	3550	0.88
			11.632	25.736	—	6051		4.82	9.48	3570	0.59
C4	0.1	298	5.882	14.965	5520	—	23.30	4.15	10.60	4930	0.89
			13.988	29.930	—	9841		4.15	10.80	5240	0.53
	10	298	5.882	14.965	5520	—	22.00	4.06	10.80	5210	0.94
			13.988	29.930	—	9841		4.06	11.00	5550	0.56

[a] a and b are respectively the radii of the polar and the equatorial axes of an oblate ellipsoid and are related to the height (L) and the diameter (d) of a cylinder by the relationship: $d = 2b$ and $L = 2a$. [b] Diffusion coefficient. Unit: 10^{10} m^2 s^{-1}. [c] Hydrodynamic radius (Å), see footnote of Table S5† for the details of calculation. [d] Hydrodynamic volume $v_H = \frac{4}{3}\pi r_H^3$ (Å). [e] Ref. 36.

DOSY experiments. In this section we investigate the effect of the decrease of the steric hindrance (at the expense of the electron acceptor ability) in the series **C1–C3** and the effect of the methoxy substitution of the CTB ring by comparing the behavior of **C1** with those of **C3** and **C4**, respectively. The data are collected in Table 1 and its complete version in the ESI (Table S5†). We also included the data that we had obtained for CTB(H,C_2H).[36] The DOSY spectra were acquired at two concentrations for each of the three complexes. We considered two models for the shape of the **C*n*** dimers, either the oblate ellipsoid or the cylinder.[42] The dimensions of these 3D figures were estimated from the computed structures of the CTBs as indicated in the ESI (Fig. S46–S53†). They were used for the calculation of the corresponding metric volumes v_M of the ellipsoid and the cylinder models. The CTBs and the corresponding cryptophane-like dimers are represented in simplified form schematically in Fig. 3. As the dimerization proceeds by interpenetration of the CTBs, two cases can be envisaged: In the first (small phosphine ligand; Fig. 3a and b), the radius a of the short axis of the ellipsoid model (distance h_{Au} between the centroids of the e-H and the Au atoms) is half the height L of the cylinder model ($2a$); in the second (Fig. 3c and d), the large phosphine substituents envelop the CTB cone. Therefore, we kept $a = h_{Au}$, but took $L = 2(h_1 - h_{Au})$, where h_1 is the height of **C*n***. In the case of CTB(H,C_2H), we considered a virtual dimer obtained by putting two such molecules concavity-to-concavity and applied the ellipsoid model. The details of the calculations of the hydrodynamic radii, hence the volumes v_H of the corresponding hydrodynamic spheres from the measured diffusion coefficients D_t are illustrated for **C4** in Fig. S54 (ellipsoid model) and S55 (cylinder model).†

Surprisingly, the v_H/v_M ratio obtained for the virtual dimer of CTB(H,C_2H) is very close to 1 (0.98), in spite of the fact that this dimer cannot exist! This result shows that the hydrodynamic behavior of the cone-shaped CTB is incidentally mimicked by the oblate ellipsoid, the metric parameters a and b of which correspond to $a = h_1$ and $b = r$ of Fig. S47.† In the case of the complexes, the ratios v_H/v_M calculated for the ellipsoid model varied between 0.84 and 1.05. However, given the results obtained in the case of the parent CTB, it is likely that the ellipsoid model is not suitable for the complexes as well. In the case of the cylinder model, the v_H/v_M ratios are all comprised between 0.50 and 0.62. They increase for **C1** by 24% (for a 11 × concentration increase), for **C3** by 10% (for a 50 × concentration increase), and for **C4** by *ca.* 6% (for a 100 × concentration increase). The cylinder model seems to be better adapted to complexes with large phosphine co-ligands, which envelop the CTB cone. Given the values of the v_H/v_M ratios

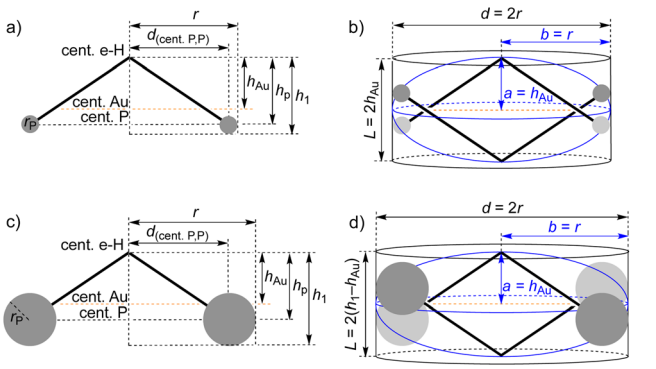

Fig. 3 Schematical views in simplified form of a CTB complex with (a) small and (c) large phosphine ligands and the corresponding (b and d) interpenetrated CTB dimers. The ellipsoid and cylinder shapes are marked with blue and black lines, respectively in (b) and (d).

obtained for **C1** and **C4** in the frame of the cylinder model, these complexes are likely to be monomeric at lower concentration. The highest rate of increase of the ν_H/ν_M ratio with concentration observed for **C1** (2.16) by comparison with **C4** (0.06) indicates that we can consider that 10 mM solutions of the former contain a small fraction of dimer in fast exchange with the monomer. Therefore, whereas ESI-MS provided evidence for dimeric species in the gas phase for all six **C*n*** complexes, solution DOSY experiments confirmed our earlier conclusion[36] that only **C1** was prone to dimerize in pure chloroform solution, albeit to a very limited extent. This was confirmed by the evolution of the ^{31}P and ^{1}H NMR spectra of solutions of **C1** in $CDCl_3$ in the concentration range 0.055–1.06 × 10^{-1} mol L^{-1} (Fig. S56†). As the concentration of **C1** increased, the signal of the PPh_3 phosphorus atom was gradually shifted to higher field and broadened, the maximum chemical shift variation in this concentration range being −0.17 ppm. The contrasted observations between NMR and ESI-MS are outward discrepancies, as the conditions of the experimental techniques (solvent, concentrations, state of the matter) are different. Moreover, the recognized risk to detect unspecific aggregates by ESI-MS must not be overlooked. This would concern, in the present case, dimers held by other interactions than those expected (here Au···Au bonds).

Investigations on the chirality of the complexes

Preparation of the enantiomerically pure complexes. CTB(OMe,C_2H) was resolved into its enantiomerically pure forms by HPLC on a chiral stationary phase, which provided (−)-CTB(OMe,C_2H) followed by (+)-CTB(OMe,C_2H). The resolution of CTB(H,C_2H) by the same means was reported earlier,[36] and afforded also (−)-CTB(H,C_2H) first, followed by (+)-CTB(H,C_2H). Polarimetric data are collected in Tables S6 (**C1–C3**) and S7 (**C4–C6**).† Whereas for (+)-CTB(H,C_2H) α_D^{25} = +633 (CH_2Cl_2, *c* = 0.121), for (−)-CTB(OMe,C_2H) it was increased in absolute value to +138 (CH_2Cl_2, *c* = 0.112). The enantiomerisation rate of CTB(OMe,C_2H) was 3.74 × 10^{-5} s^{-1} (62 °C, $CHCl_3$), which is *ca.* 25 times higher than the value found for CTB(H,C_2H), 1.40 × 10^{-6} s^{-1} (40 °C, CH_2Cl_2). The corresponding energy barriers are 110.8 kJ mol^{-1} (26.5 kcal mol^{-1}) and 111.9 kJ mol^{-1} (26.7 kcal mol^{-1}). Therefore the methoxy substituents increase only by 1% the enantiomerisation barrier of the CTB. In any case the latter is in the 26–28 kcal mol^{-1} range noted for this family of compounds.[29]

The resolution of the CTB complexes by chiral HPLC was not as straightforward, because in most cases the compounds were prone to partial decomposition upon elution through the column. Separation of the enantiomers by chiral HPLC was restricted to **C1**, affording (+)-**C1** and (−)-**C1**, as reported earlier;[36] **C5**, which afforded (−)-**C5** then (+)-**C5**; and **C6**, which afforded (+)-**C6** then (−)-**C6**. However, the enantiopurity of (+)-**C6** was not satisfactory. The enantiomers of the remaining complexes (**C2**, **C3**, and **C4**) were prepared separately from the enantiopure CTB precursors using the mild (short reaction time, room temperature) reaction conditions of method B. Accordingly, (−)-**C2** and (+)-**C2** were obtained in 79 and 41% yields, (−)-**C3** in 73% yield, and (−)-**C4** and (+)-**C4** in 86 and 56% yields, respectively. Additionally, (−)-**C5** on the one hand, (−)-**C6** and (+)-**C6** on the other hand were also prepared by method B and obtained in 80, 70, and 61% yields, respectively (Table S1†).

Electronic and chiroptical properties – absolute configurations. The electronic absorption and ECD spectra of the compounds of this study are shown in Fig. S57–S69.† The electronic absorption spectrum of CTB(H,C_2H) in CH_2Cl_2 (Fig. S57b†) shows a prominent broad band with strong absorptions in the 230–265 nm region with a broad maximum at 247 nm (ε = 55 700 mol^{-1} cm^{-1}) and a sharp maximum at 257 nm (ε = 57 800 mol^{-1} cm^{-1}), and a weak broad band in the 265–310 nm region with maxima at 282 nm (ε = 2500 mol^{-1} cm^{-1}) and 293 nm (ε = 2050 mol^{-1} cm^{-1}). The two bands correspond to the B_{1u} and B_{2u} forbidden transitions of the benzene ring, respectively. They are shifted bathochromically by *ca.* 10 nm with respect to *m*-ethynyltoluene (Fig. S57a†). The magnitude and sign of the spectroscopic moment *sm* of the ethynyl substituent for the so-called 2600A electronic transition of benzene was estimated to +19 (pp. S5–S6†). The ECD spectrum of CTB(H,C_2H) (Fig. 4a and S57b†) shows a bisignate Cotton effect in the B_{1u} region, with a broad and prominent band up to 257.9 nm and a weaker band extending between

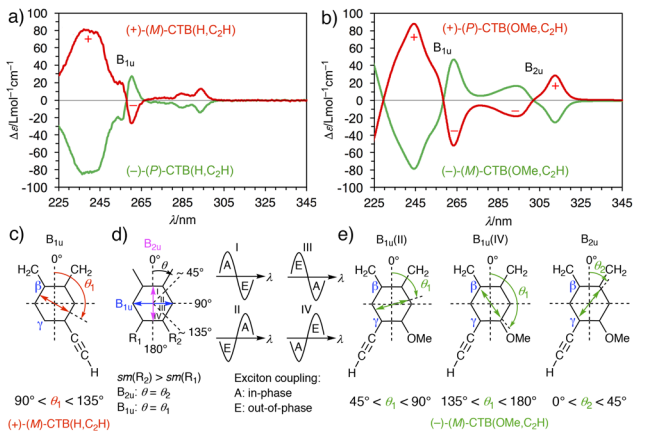

Fig. 4 Plots of the ECD spectra of (a) CTB(H,C_2H) in CH_2Cl_2 and (b) CTB(OMe,C_2H) in CH_3CN between 225 and 345 nm, which covers the regions of the B_{1u} and B_{2u} transitions. The ECD spectrum of CTB(OMe,C_2H) in the full range is shown in Fig. S64b.† The spectra of the first eluted enantiomers are in green, those of the second eluted enantiomers are in red. In (c) and (e) are represented the directions of polarization (angle θ_1) of the B_{1u} transitions of (*M*)-CTB(H,C_2H) and (*M*)-CTB(OMe,C_2H). Two are possible in the case of the latter compounds. They are discussed in the text. In (e) is also represented the direction of polarization (angle θ_2) of the B_{2u} transition of (*M*)-CTB(OMe,C_2H). It is lacking for the B_{2u} transition of (*M*)-CTB(H,C_2H), because this transition does not show an exciton couplet. (d) The orientations of the dipole moments of the transitions B_{1u} and B_{2u} of benzene are shown in blue and pink, respectively. The expected shapes of the exciton couplets of the B_{1u} and B_{2u} transitions as a function of the location of the direction of polarization of the transition dipole in quadrants I (0° < θ < 45°), II (45° < θ < 90°), III (90° < θ < 135°), and IV (135° < θ < 180°) are also shown. See ref. 43 and 46 for details.

257.9 and 266.3 nm. In the B_{2u} region, the ECD spectrum, extending between 266.3 nm to *ca.* 303 nm shows a singly signed band and is even weaker. Simulation of the ECD of (*M*)-CTB(H,C_2H) by TD-DFT calculations at the CAM-B3LYP-D3 6-311+G(d,p) level of theory (Fig. S59†) indicated that this enantiomer was the second eluted, and thus corresponded to (+)-CTB(H,C_2H); therefore (*P*)-CTB(H,C_2H) is (−)-CTB(H,C_2H).

The electronic absorption spectrum of CTB(OMe,C_2H) in acetonitrile (Fig. S63a†) shows three bands, a high energy band with a maximum at 216 nm (ε = 68 700 mol^{-1} cm^{-1}), an intermediate energy band with a maximum at 247 nm (ε = 48 500 mol^{-1} cm^{-1}) and a shoulder at 253 nm (ε = 46 300 mol^{-1} cm^{-1}), and a low energy band with a shoulder at 303 nm (ε = 15 300 mol^{-1} cm^{-1}), a maximum at 310 nm (ε = 17 100 mol^{-1} cm^{-1}), and a tail extending from *ca.* 320 nm down to *ca.* 400 nm. The high energy band corresponds to the allowed E_{1u} transition of the benzene rings, and the intermediate energy bands are located in the B_{1u} region, whereas the low energy band is located in the B_{2u} region. By contrast with CTB(H,C_2H), the ECD spectrum of CTB(OMe,C_2H) in acetonitrile (Fig. 4b and S64b†) shows three bisignate exciton patterns. The highest energy one is centered on the isotropic absorption of the E_{2u} transition, and the lowest energy ones are centered on the isotropic absorptions of the B_{1u} and B_{2u} transitions. In the B_{1u} region, a bisignate Cotton effect between 229.5 and 276 nm with sign inversion at 258.4 nm, is followed, in the B_{2u} region, by a bisignate Cotton effect showing the opposite sequence of signs from 276 to *ca.* 350 nm with sign inversion at 302.2 nm. Simulation of the ECD of (*P*)-CTB(OMe,C_2H) by TD-DFT calculations at the CAM-B3LYP-D3 6-311+G(d,p) level of theory (Fig. S65†) indicated that this enantiomer was the second and thus corresponded to (+)-CTB(OMe,C_2H); therefore the absolute configuration of (+)-CTB(OMe,C_2H) is (*P*)-CTB(OMe,C_2H), and the one of (−)-CTB(OMe,C_2H) is (*M*)-CTB(OMe,C_2H).

The simulation of the ECD spectra of CTBs has been, in the past, undertaken by Collet, Gottarelli and coworkers[43–45] in the frame of the Kuhn-Kirkwood coupled-oscillator theory, in which the exciton model for molecules incorporating chromophores interacting through their electric transition dipoles generated in a radiation field was developed (see Fig. 4d). The CTBs contain three benzene chromophores that are tilted around a C_3 symmetry axis. Each benzene ring bears four substituents, invariably two methylene bridges in β and β′ positions, and two variable substituents R and R′ in γ and γ′ positions. The lowest energy transitions in the UV are labelled B_{1u} (230–250 nm) and B_{2u} (255–310 nm); if R = R′ their dipole moments are polarized along the long and short axes of the benzene ring, respectively. If R ≠ R′, the transition dipole moments are tilted by an angle of θ_1 (for B_{1u}) or θ_2 (for B_{2u}), as shown in Fig. 4c and e. The sign and magnitude of θ_2 depends on the values of the spectroscopic moments *sm* of R and R′. θ_1 often equals θ_2 + 90° but this turned out not to be always the case.[46,47] Three coupling modes for each of the B_{2u} and B_{1u} transitions operate in C_3-symmetric CTBs, the symmetrical A-coupling and the two degenerate non-symmetrical E-couplings. In A the electric (μ) and magnetic (m) moments are aligned along the C_3 axis whereas in E they are polarized along the direction perpendicular to the C_3 axis. Each of the A and E couplings generate one of the two oppositely signed Cotton bands of the exciton CD, the sign of which directly depends on the sign of the rotational strength $\mu \times m$, and the energy of which depends on the nature of the interactions between the dipoles (higher if repulsive, lower if attractive).

The ECD spectra of CTB(H,C_2H) and CTB(OMe,C_2H) were examined in the light of the exciton coupling theory. The former showed a bisignate pattern only in the B_{1u} region with a positive-negative sequence from high to low energy (negative Cotton effect) for the *M* enantiomer. It corresponds therefore to the E–A sequence of couplings of quadrant III, which is in agreement with our finding that *sm*(C_2H) = 19 > *sm*(H) = 0 $M^{-1/2}$ $cm^{-1/2}$. CTB(OMe,C_2H) showed bisignate patterns for the B_{1u} (positive Cotton effect) and the B_{2u} transitions (negative Cotton effect) for the *M* enantiomer. The pattern of the B_{2u} transition corresponds to the A–E sequence of couplings of quadrant I, which is in agreement with the fact that *sm*(C_2H) = 19 < *sm*(OMe) ≈ 31 $M^{-1/2}$ $cm^{-1/2}$.[48] By contrast, the B_{1u} transition should show a negative Cotton effect (quadrant III) if the relationship: $\theta_1 = \theta_2 + 90°$ applied. As a positive Cotton effect is observed, the B_{1u} and B_{2u} transitions are not polarized at 90°. Therefore, the direction of polarization of the B_{1u} transition is either located in quadrant I (B_{1u}(II) of Fig. 4e), or in quadrant IV (B_{1u}(IV) of Fig. 4e) as they both account for the observed positive Cotton effect. This confirms the observation by Collet and coworkers that only the B_{2u} transition can be used safely in the case of CTB(OMe,C_2H) for the absolute configuration assignment.[46]

The electronic absorption and chiroptical properties ($[\alpha]_\lambda^{25}$, electronic circular dichroism – ECD) of the enantiopure complexes, *i.e.*, (−)-**C2** and (+)-**C2** (Fig. S62†), (−)-**C3** and (+)-**C3** (Fig. S63†), (−)-**C4** and (+)-**C4** (Fig. S66†), (−)-**C5** and (+)-**C5** (Fig. S68†), and (−)-**C6** and (+)-**C6** (Fig. S69†) were recorded using solutions in CH_2Cl_2, and the data are collected in Tables S6–S8† together with those of (−)-**C1** and (+)-**C1** (Fig. S60†), which were available from a previous study.[36] The electronic absorption spectra of **C1–C3** in CH_2Cl_2 all show the same pattern, a strong absorption band at high energy, which is characterized by a shoulder at *ca.* 236 nm (ε = 112 600 M^{-1} cm^{-1}), and a broad structured band extending between 255 and 315 nm, which, in the case of **C1**, shows a shoulder at 263 nm (ε = 56 500 M^{-1} cm^{-1}), maxima at 275 (82 000), 285 (97 500), and 297 nm (ε = 83 900 M^{-1} cm^{-1}), and a shoulder at 306 nm (ε = 39 200 M^{-1} cm^{-1}). There is a weak residual absorption extending down to *ca.* 350 nm. The spectra undergo a hypochromic (**C1** > **C2** ∼ **C3**) and a slight hypsochromic (*ca.* 1 nm) shift upon going from **C1** to **C3**, the differences being the highest in the high energy region.

The ECD spectra of **C1–C3** (Fig. 5a) show similar patterns: from high to low energy, in the B_{1u} region, a bisignate non-symmetrical band, the highest energy and absorbance component extending down to *ca.* 264 nm, followed by an intermediate energy and weak absorbance component across

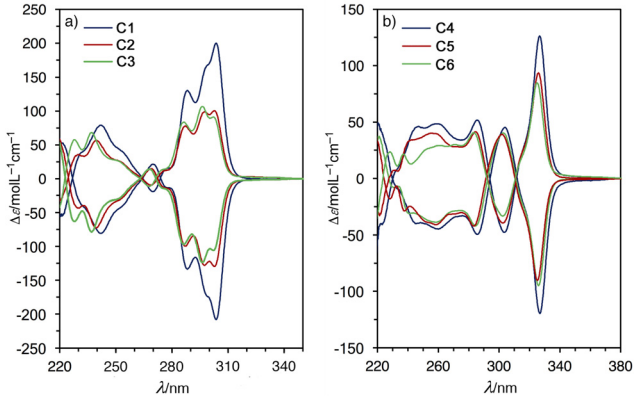

Fig. 5 Plots of the ECD spectra of (a) complexes **C1–C3** and (b) complexes **C4–C6** in CH_2Cl_2.

10 nm; in the B_{2u} region, a singly signate band between 274 and 315 nm tailing down to 350 nm. The broadest bands are structured, which is particularly clear in the case of **C3**. Upon going from **C1** to **C3**, these maxima (in absolute value) undergo hypsochromic (*ca.* 1–3 nm) and hypochromic (**C1** > **C2** ~ **C3**) shifts. The ECD spectrum of (*M*)-**C1** was simulated by TD-DFT calculations (Fig. S61†). Comparison of the simulation shows that it reproduces the sequence of signs and number of bands of the experimental spectrum of the second eluted enantiomer, (+)-**C1**. Therefore, (*P*)-**C1** is (−)-**C1**.

The electronic absorption spectra of **C4–C6** show three bands as for the parent CTB(OMe,C_2H). For example, in the case of **C4**, from the highest to the lowest energy: the foot of an intense band, then an intermediate energy structured band with three local maxima of similar absorbance (263, 268, and 275 nm), and peaking at 284 nm (ε = 59 100 M^{-1} cm^{-1}), followed by a low energy structured band with a shoulder at 315 nm (ε = 48 600 M^{-1} cm^{-1}) and a maximum at 324 nm (ε = 58 800 M^{-1} cm^{-1}), with a tail extending between 340 and 400 nm. As observed in the case of the series **C1–C3**, upon going from **C4** to **C6**, the maxima slightly shift to lower energy, and the absorbance of **C4** is much higher than those of **C5** and **C6**.

The ECD spectra of the complexes **C4–C6** (Fig. 5b) show the same sequence of bands as for **C1–C3**: in the case of **C4**, from high to low energy, a broad structured band between 229.8 and 294.1 nm, then a band of opposite sign with a single maximum at 304 nm extending down to *ca.* 312 nm, and in the low energy region, after sign inversion, a band peaking at 327 nm, showing the highest differential absorbance. The local maxima show a slight hypsochromic shift within the sequence **C4–C6**. The hypochromic shifts are less marked than in the **C1–C3** series. The ECD spectrum of (*P*)-**C4** was simulated by TD-DFT calculations (Fig. S67†). Comparison of the theoretical and experimental data shows that the calculated spectrum of (*P*)-**C4** coincides with the experimental spectrum of (+)-**C4**. Therefore (*P*)-**C4** is (+)-**C4** and (*M*)-**C4** is (−)-**C4**. Given the invariance of the Cotton effects within the homogeneous series **C1–C3** and **C4–C6** each, (*M*)-**C*n*** ⇔ (+)-**C*n*** and (*P*)-**C*n*** ⇔ (−)-**C*n*** for *n* = 1–3, and (*M*)-**C*n*** ⇔ (−)-**C*n*** and (*P*)-**C*n*** ⇔ (+)-**C*n*** for *n* = 4–6. It is worth noticing that the same relationships hold true for CTB(H,C_2H) and CTB(OMe,C_2H).

General interpretation of the electronic absorption and ECD spectra of C1–C6

The high energy absorptions (230–265 nm for **C1–C3**, 230–320 nm for **C4–C6**) arise from intraligand transitions of the coordinated alkynyl CTB and phosphine ligands. In particular, the decrease of the absorption between 230 and 260 nm upon going along both series is due to the decrease of the number of phenyl substituents in the series PPh_3 > PPh_2Me > $PPhMe_2$. The lower energy absorption bands (265–350 nm for **C1–C3**, 300–400 nm for **C4–C6**) were attributed in previous studies to gold(I)-perturbed intraligand $\pi \rightarrow \pi^*$ (C≡CAr) transitions of the alkynyl units[49,50] and σ(Au–P) → π* (C≡C) transitions.[51] Vibrational progressional spacings between 1276 and 1659 cm^{-1} (aromatic C=C stretches)[52] were calculated in the 260–300 nm regions of **C1** and **C4**, whereas a vibrational progressional spacing of *ca.* 2100 cm^{-1} (C≡C stretch) was calculated in the same region for **C4**.[53] The three chromophores in **C1** are independent, as the molar extinction coefficient of this complex at 285 nm (94 100 M^{-1} cm^{-1}) is three times the one measured for the mononuclear complex $Ph_3PAuC{\equiv}CPh$.[50] The slight blue shift of the absorption maxima upon moving along the series **C1–C3** on the one hand, **C4–C6** on the other hand, confirms that these absorption features may involve the σ(Au–P) orbital, as its stabilization by the gradual replacement of a phenyl by a methyl substituent makes transitions originating therefrom highest in energy.

The ECD pattern of the spectra of **C1–C3** is similar to, but red shifted by *ca.* 5–10 nm with reference to the one of CTB(H,C_2H), with a bisignate Cotton effect in the B_{1u} region between 225 and 275 nm, and a considerably enhanced singly signed Cotton effect in the B_{2u} region. The sequence of signs in the B_{1u} region is the same along the series CTB(H,C_2H), **C1–C3**, which implies that the metallation of the alkynyl substituent does not change its *sm* ($90 < \theta_1 < 135$). The ECD pattern of the spectra of **C4–C6** differs, at first glance, from the one of CTB (OMe,C_2H), unless we consider that the low energy Cotton band of the B_{1u} couplet has merged with the high energy band of the B_{2u} couplet, due to a stronger red shift of the former with respect to the latter. If this hypothesis is correct, the low energy Cotton band of the B_{2u} couplet is considerably enhanced, as in the case of the former series, and its sequence of signs is preserved, which allows us to draw the same conclusions about the *sm* of the metallated alkynyl substituents.

Study of the phosphine exchange in the gas phase in C1–C6

Exchange of phosphine ligands of mononuclear phosphine-gold ethynyl complexes has been investigated in solution by ^{31}P NMR spectroscopy and shown to be fast.[38] Inspired by reports on the use of ESI-MS to study the exchange of components in metallo-supramolecular macrocycles[54] and cages,[55]

we examined how this technique can bring some information on the phosphine exchange reactions within the series of alkynylgold(I) phosphine complexes **C1–C6**. As each species is characterized by a single signal, the spectra of the mixtures are quite simple, making quantifications straightforward. The equilibrium pertaining to the phosphine exchange reaction between two complexes **Cp** and **Cq** is the following (eqn (1)):

$$\mathbf{Cp} + \mathbf{Cq} \rightleftarrows \mathbf{Cp}' + \mathbf{Cq}' \quad (1)$$

in which CTBs **Cp**′ and **Cq**′ result from the replacement of a phosphine of CTB **Cp** by a phosphine of CTB **Cq** and *vice versa*. We can define the equilibrium constant $K_{(\mathbf{Cp},\mathbf{Cq})}$ according to the eqn (2):

$$K_{(\mathbf{Cp},\mathbf{Cq})} = \frac{[\mathbf{Cp}' + \mathrm{H}^+]}{[\mathbf{Cp} + \mathrm{H}^+]} \times \frac{[\mathbf{Cq}' + \mathrm{H}^+]}{[\mathbf{Cq}' + \mathrm{H}^+]}, \quad (2)$$

in which [**C*n*** + H^+] is the concentration of protonated **C*n***, measured as the relative intensity of its ESI-MS signal.

The nine following pairs {**Cp**, **Cq**} of CTBs were examined: {**C1**, **C2**}, {**C1**, **C3**}, {**C1**, **C4**}, {**C2**, **C3**}, {**C2**, **C5**}, {**C3**, **C6**}, {**C4**, **C5**}, {**C4**, **C6**}, and {**C5**, **C6**}. Except for the pairs {**C1**, **C4**}, {**C2**, **C5**}, and {**C3**, **C6**}, in which the **Cp** and **Cq** complexes contain the same phosphine ligand, that is, PPh_3 for {**C1**, **C4**}, PPh_2Me for {**C2**, **C5**}, and $PPhMe_2$ for {**C3**, **C6**}, and give rise to degenerate exchange reactions, these experiments allowed us to observe new signals that could not be detected when a single complex was examined, that is, signals resulting from the exchange of a phosphine, *e.g.* [**Cp**′ + H^+] = [**Cp**-$PPh_nMe_{(3-n)}$ + $PPh_nMe_{(3-n)}$ + H^+, and signals arising from the diprotonated heterodimer, *e.g.* [**Cp** + **Cq** + 2H]$^{2+}$. Therefore, for a given {**Cp**, **Cq**} pair, we monitored the signal intensities of the following species as a function of E_{coll}: the singly charged species [**Cp** + H^+, [**Cq** + H^+, [**Cp**′ + H^+, [**Cq**′ + H^+, and the doubly charged species [2**Cp** + 2H]$^{2+}$, [2**Cq** + 2H]$^{2+}$, [**Cp** + **Cq** + 2H]$^{2+}$, [2**Cp**′ + 2H]$^{2+}$, [2**Cq**′ + 2H]$^{2+}$, [**Cp** + **Cp**′ + 2H]$^{2+}$ and [**Cq** + **Cq**′ + 2H]$^{2+}$. The spectra and the corresponding plots of the relative proportion of each species as a function of E_{coll} are collected in Fig. S70–S87,† the spectra of {**C4**, **C5**} being also reproduced in Fig. 6.

It must be emphasized that the relative proportions of the different species are those of the protonated CTBs, which are detected in this form. Therefore they *a priori* depend on the relative basicities (electron richness) of the complexes. We expect that it is stronger in the case of the methoxy-substituted series (**C4–C6**) and, within each series, it increases with the degree of methyl-substitution of the phosphine, which was roughly observed in the case of the experiments run on each complex alone (see Fig. 2). Moreover, the basicity of **Cp** and **Cp**′ (respectively **Cq** and **Cq**′) should differ in the following way: if $p < q$, the basicity of **Cp**′ should be higher than the basicity of **Cq**′, and the basicity of **Cq**′ should be lower than the basicity of **Cq**, and *vice versa* if $p > q$.

Examination of the nine plots shows that the populations of the doubly charged, dimer species decrease as E_{coll} increases, while the populations of the singly charged,

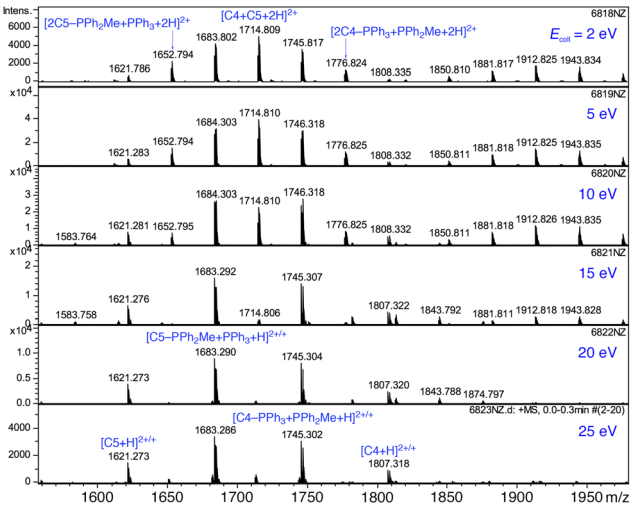

Fig. 6 Evolution of the ESI-MS spectra of a 1 : 1 mixture of 10^{-4} M solutions of complexes **C4** and **C5** in $CHCl_3$/i-PrOH/HCO_2H 50 : 49.5 : 0.5.

monomer species, that is, [**Cp**′ + H^+, [**Cq**′ + H^+, [**Cp** + H^+, and [**Cq** + H^+, increase concomitantly. The E_{coll} at which the former approach their minimum roughly coincides with the E_{coll} at which the latter approach their maximum, between 10 and 15 eV. Another general trend is the highest proportion of species containing two different phosphines, *e.g.* [**Cp**′ + H^+ *vs.* [**Cp** + H^+ and [2**Cp**′ + 2H]$^{2+}$ *vs.* [2**Cp** + 2H]$^{2+}$. These differences result from the decrease of the concentrations of **Cp** and **Cq**, as **Cp**′ and **Cq**′ are generated, as explicited in the equilibrium (1).

The differences between the signals of **Cp** and **Cq** on the one hand, and of **Cp**′ and **Cq**′ on the other hand, are usually minimal at low E_{coll} (5 eV), then they increase with E_{coll}. This is particularly the case of the pairs {**C1**, **C3**}, {**C4**, **C5**}, {**C4**, **C6**}, and {**C5**, **C6**}. The other non-degenerate pairs {**C1**, **C2**} and {**C2**, **C5**} illustrate two opposite behaviors, as for the former these differences are low, whatever E_{coll}, and for the latter they are high, whatever E_{coll}.

We consider first in detail the case of the pairs of complexes {**C1**, **C4**}, {**C2**, **C5**}, and {**C3**, **C6**}, giving degenerate exchange reactions (Fig. S74, S75 and S78–S81†). The relative proportions within each pair follow the order [**C1** + H^+ > [**C4** + H^+, [**C2** + H^+ ≈ [**C5** + H^+, and [**C3** + H^+ ≫ [**C6** + H^+, which are opposite the expected trends, at least for the pairs {**C1**, **C4**} and {**C3**, **C6**}. Meanwhile, in the case of the pairs {**C1**, **C4**} and {**C2**, **C5**}, at E_{coll} < 10 eV, the signals of highest intensity originate from the dimer species [**C1** + **C4** + 2H]$^{2+}$ > [2**C4** + 2H]$^{2+}$ ≫ [2**C1** + 2H]$^{2+}$ for the former pair, and [**C2** + **C5** + 2H]$^{2+}$ > [2**C5** + 2H]$^{2+}$ ≫ [2**C2** + 2H]$^{2+}$ for the latter pair, the intensities of the signals of [2**C1** + 2H]$^{2+}$ and [2**C2** + 2H]$^{2+}$ being the weakest of all the species detected. Therefore, in the case of the homodimers, the order of the signal intensities follows the expected CTB basicities. The plots of Fig. S75 and S79† nicely illustrate the fact that the dimers [2**C4** + 2H]$^{2+}$ and [2**C5** + 2H]$^{2+}$ play the role of reservoir of **C4** and **C5**, respectively, and

that $[2\mathbf{C4} + 2H]^{2+} \gg [2\mathbf{C1} + 2H]^{2+}$ compensates for $[\mathbf{C1} + H]^+ > [\mathbf{C4} + H]^+$, while $[2\mathbf{C5} + 2H]^{2+} \gg [2\mathbf{C2} + 2H]^{2+}$ compensates for $[\mathbf{C2} + H]^+ \approx [\mathbf{C5} + H]^+$ at least at $E_{coll} \leq 15$ eV. Taking into account the dimers restores the order expected on basicity grounds. In the case of the {**C3**, **C6**} pair, the observed $[\mathbf{C3} + H]^+ \gg [\mathbf{C6} + H]^+$ order is consistent with the ranking deduced from subjecting separately **C3** and **C6** to the ESI-MS experiments, as shown in Fig. 2, which could suggest that other factor(s) than basicity could contribute to the singular behavior of **C6**.

We now turn to the six pairs giving non-degenerate exchange reactions. In the case of {**C1**, **C2**} (Fig. S70 and S71†) the differences between the apparent proportions of $[\mathbf{C1} + H]^+$ and $[\mathbf{C2} + H]^+$ (and of $[\mathbf{C1}' + H]^+$ and $[\mathbf{C2}' + H]^+$) are small and in keeping with the observations done on the individual complexes (Fig. 2). As a consequence, the ratios $[\mathbf{Cp}' + H]^+/[\mathbf{Cp} + H]^+$ are similar, and at 20 eV, where only these four species remain, we can calculate the equilibrium constant as shown in eqn (3):

$$K_{(\mathbf{C1},\mathbf{C2})} = \frac{[\mathbf{C1}' + H^+]}{[\mathbf{C1} + H^+]} \times \frac{[\mathbf{C2}' + H^+]}{[\mathbf{C2} + H^+]} = 9.2 \quad (3)$$

Switching to the homologous system in the other series, that is, {**C4**, **C5**} (Fig. S82 and S83†) shows substantial differences between the responses of **C4** and **C5**. However, they are now in agreement with the expected basicity order, the signals arising from **C5** being more intense than those arising from **C4**. However, as the ratios $[\mathbf{Cp}' + H]^+/[\mathbf{Cp} + H]^+$ differ by 30% at 20 eV, it is not possible to determine an equilibrium constant for this system. Back to the unsubstituted series, we examine the two systems {**C1**, **C3**} (Fig. S72 and S73†) and {**C2**, **C3**} (Fig. S76 and S77†). The responses of the CTBs are fully consistent with the basicity order **C3** > **C2** > **C1**, but the differences in the ratios $[\mathbf{Cp}' + H]^+/[\mathbf{Cp} + H]^+$ for each pair again preclude their use for the calculation of equilibrium constants. Finally, we examined the cases of the systems homologous of {**C1**, **C3**} and {**C2**, **C3**} in the methoxy-substituted series, that is, {**C4**, **C6**} (Fig. S84 and S85†) and {**C5**, **C6**} (Fig. S86 and S87†). **C4**′ and **C6**′ are not distinguished from each other whatever the E_{coll} value, but the response of **C4** is stronger than the response of **C6** at $E_{coll} > 2$ eV, that is opposite the one expected from their basicity order. Nevertheless, **C4** and **C6** give signals of relatively close intensities at 20 eV, which allowed us to estimate the equilibrium constant as shown in eqn (4):

$$K_{(\mathbf{C4},\mathbf{C6})} = \frac{[\mathbf{C4}' + H^+]}{[\mathbf{C4} + H^+]} \times \frac{[\mathbf{C6}' + H^+]}{[\mathbf{C6} + H^+]} = 6.2 \quad (4)$$

The differences between the responses of **C5** and **C6** on the one hand, and of **C5**′ and **C6**′ on the other hand, are also opposite the expected basicity order **C6** > **C5**, but they are too high to allow us to calculate an equilibrium constant. The fact remains that the observed inversions affect all three CTB pairs involving **C6**, that is {**C3**, **C6**}, {**C4**, **C6**}, and {**C5**, **C6**}, which also confirms the singularity of **C6**.

Conclusions

Organometallic cyclotribenzylenes, in particular those containing gold, are novel chiral compounds, the properties of which deserve being investigated further. In this work, we have investigated methods and selected the best for their preparation in enantiomeric pure form. Their electronic absorption and ECD bands, shifted to the red by gold complexation, can be tuned by the nature of the substituents of the CTB platform. The complexes are mainly monomeric in solution, according to DOSY experiments. We have shown, by ESI-MS, that the ability of the CTB complexes to form proton adducts was dependent upon the nature of the phosphine and CTB substitution, the more basic the complex, the stronger the signal of the protonated species. ESI-MS was also used to probe phosphine exchange reactions. Future work will explore the emission properties of these alkynylgold complexes. In addition, as they encompass a cavity lined by phosphine termini of different sizes, we plan to screen potential guests and study the kinetics and thermodynamics of their interaction with the guests discovered.

Experimental

Materials, methods and instrumentation

The following abbreviations were used: THF (tetrahydrofuran) and DMF (*N*,*N*-dimethylformamide). Unless otherwise stated, all reactions were performed under argon using the following solvents and liquid reagents, which were dried and distilled under argon: DMF (anhydrous magnesium sulfate), THF (Na/benzophenone), dichloromethane (P_2O_5), methanol (Mg), triethylamine (KOH), and acetone (K_2CO_3). Other commercially available solvents and reagents were used as received. Separations by flash column chromatography used silicagel (Geduran Si 60, 40–63 μm from Merck). CTB(H,C_2H),[36] **C1**, (+)-**C1** and (−)-**C1**,[36] CTB(OMe,C_2H),[37] and [Au(PPh$_n$Me$_{3-n}$)Cl], n = 1, 2, and 3,[56] were obtained according to the literature. $[CTB(H,C_2Au)]_n$ and $[CTB(OMe,C_2Au)]_n$ were prepared in racemic and enantiomeric pure forms by using reported procedures.[41] NMR spectra were recorded on Bruker Avance III 400 MHz and Avance II 500 MHz spectrometers. Chemical shifts were reported using the residual solvent ^{1}H signal (7.26 and 77.16 ppm for $CHCl_3$) as internal reference for ^{1}H NMR and ^{13}C NMR, respectively, and the phosphorus signal (set at 0 ppm) of 85% H_3PO_4 placed inside an insert for ^{31}P NMR. IR spectra were recorded using a Bruker Alpha II FT-IR spectrometer. **CAUTION**: Some gold acetylide have been reported to be shock sensitive. These compounds should be handled in small quantities using protective equipment.

Analytical and preparative chiral HPLC

Chiral HPLC analyses were performed using the Agilent 1260 Infinity unit (pump G1311B, autosampler G1329B, DAD G1315D) with Igloo-Cil ovens, monitored by SRA Instruments Seleccol software. The chiroptical detection was performed

with Jasco OR-1590 and CD-2095 polarimetric and circular dichroism detectors, respectively. The signs given by the on-line circular dichroïsm at 254 nm and the polarimeter are the signs of the compound in the solvent used for the chromatographic separation. HPLC grade heptane and isopropanol were degassed and filtered on a 0.45 μm millipore membrane before use. Retention times R_t (min), retention factors $k_i = (R_{ti} - R_{t0})/R_{t0}$, enantioselectivity factors $\alpha = k_2/k_1$, and resolution $R_s = 1.18(R_{t2} - R_{t1})/(w_1 + w_2)$ were determined (R_{t0} was measured by injection of 1,3,5-tri(*tert*-butyl) benzene and w_i is the peak width at half-height). Preparative chiral HPLC separation were performed using an Agilent 1260 Infinity unit (pump G1311C, autosampler G1329B, DAD G1365D and fraction collector G1364C), monitoring with an Agilent OpenLAB CDS Chemstation LC.

Mass spectrometry

Mass data were obtained using a MicrOTOF-Q II (Bruker Daltonics, Bremen, Germany) mass spectrometer fitted with Z-spray electrospray ion source and with a mass range of 2–4000 Thomson. The mass spectrometer was operated in positive ion mode, with a potential of 3500 V applied to the electrospray probe body and the source temperature set to 180 °C. MS data were acquired from 300 to 3000 *m*/*z*. The ISCID energy was kept at 0 eV, while energy of the collision cell (E_{coll}) was varied from 2 to 20 eV in order to dissociate potential dimers. Mass calibration was performed using a mix of Tune Low (Agilent Technologies G1969-8500) prior to analysis. Data were processed with Data Analysis software (Bruker Daltonics). CTB solutions at a concentration of 10^{-4} mol L^{-1} in $CHCl_3$ were diluted to a final concentration of 5×10^{-5} mol L^{-1} with an equal volume of isopropanol acidified with HCO_2H 1%, so that the composition of the sample mixture was $CHCl_3$/^{i}PrOH/HCO_2H 50 : 49.5 : 0.5 prior to injection into the mass spectrometer.

Preparation and characterization of CTB(R,C_2AuPPh$_n$Me$_{3-n}$) C2–C6

Method A. CTB(R,C_2H), [AuCl(PPh$_n$Me$_{3-n}$)], and sodium methoxide were mixed in THF and methanol (1 : 1, v/v) at 40 °C. After stirring the reaction mixture for several days, the solvents were removed by rotary evaporation. The residue was taken up in dichloromethane, and clarified by filtration, which afforded a yellow solution. The latter was concentrated to a volume of 1–2 mL and treated by dropwise addition of cyclohexane (1.5–2 mL) until the product started to precipitate. The mixture was stored in the refrigerator overnight and filtered. A yellow powder was obtained after drying in vacuum.

Method B. A solution of PPh$_n$Me$_{3-n}$ in THF was added to a suspension of [CTB(OMe,C_2Au)]$_n$ in dichloromethane, and the reaction mixture stirred for the given period of time at room temperature. It was then clarified by filtration through a porosity 4 sintered glass funnel, which afforded a light-yellow solution. The solvents were evaporated to dryness. The solid residue was washed with methanol and dried in vacuum, leaving a yellow powder.

C2. (Method A) Prepared from CTB(H,C_2H) (0.005 g; 0.0146 × 10^{-3} mol), [AuCl(PPh$_2$Me)] (0.019 g; 0.0439 × 10^{-3} mol), and sodium methoxide (0.012 g; 0.222 × 10^{-3} mol) in MeOH (4 mL) and THF (4 mL), 3 days stirring. Yield: 0.0095 g (0.0063 mol, 43%). (Method B) Prepared from PPh$_2$Me (0.016 mL, 0.0173 g; 0.0862 × 10^{-3} mol) and [CTB(H,C_2Au)]$_n$ (0.026 g; 0.0279 × 10^{-3} mol), in CH_2Cl_2 (3 mL) and THF (1 mL), 1.5 h stirring. Yield: 0.036 g (0.0235 × 10^{-3} mol, 84%). Mp 195 °C; ^{1}H NMR (500.13 MHz, $CDCl_3$, 295 K): δ (ppm) = 7.636 (m, 12 H; *o*- and *o*′-H), 7.490 (d, $^4J_{H,H}$ = 1.5 Hz, 3 H; α′-H), 7.453 (m, 6 H; *p*-H), 7.439 (m, 12 H; *m*- and *m*′-H), 7.247 (d, $^3J_{H,H}$ = 8.0 Hz, 3 H; α-H), 7.186 (dd, $^4J_{H,H}$ = 1.5 Hz, $^3J_{H,H}$ = 7.5 Hz, 3 H; γ-H), 4.742 (d, $^2J_{H,H}$ = 13.5 Hz, 3 H; a-H), 3.624 (d, $^2J_{H,H}$ = 13.5 Hz, 3 H; e-H), 2.052 (d, $^2J_{H,P}$ = 9.0 Hz; CH_3); ^{13}C NMR (125.77 MHz, $CDCl_3$, 295 K): δ (ppm) = 138.82 (s; β′-C), 138.15 (s; β-C), 134.14 (s; α′-C), 132.97 (d, $^2J_{C,P}$ = 13.8 Hz; *o*- and *o*′-C), 131.72 (d, $^1J_{C,P}$ = 55.3 Hz; i-C), 131.58 (s; *p*-C), 131.00 (s; γ-C), 130.25 (s; α-C), 129.27 (d, $^3J_{C,P}$ = 11.3 Hz; *m*- and *m*′-C), 123.40 (s; γ′-C), 104.71, 104.48 (2 s; δ′- and ε′-C), 37.04 (s; CH_2), 14.24 (d, $^1J_{C,P}$ = 35.2 Hz; CH_3); ^{31}P NMR (161.98 MHz, $CDCl_3$, 298 K): δ (ppm) = 27.19 (s); IR (KBr): ν (cm^{-1}) = 3053 (w), 3019 (w), 2958 (sh), 2922, 2854 (m), 2352 (w), 2319 (w), 2103, 1968, 1892 (w), 1600 (m), 1545 (w), 1486 (m), 1434 (s), 1417, 1385, 1334, 1310 (m), 1294 (w), 1267, 1239 (m), 1204 (sh), 1189, 1162 (m), 1102 (s), 1075 (sh), 1030 (w), 1002 (m), 970 (sh), 957 (m), 890 (s), 834 (m), 807 (w), 737 (s), 690 (s), 635 (m), 483, 475, 427 (w), 511 (s), 478 (m), 453 (sh), 431 (sh); HR-MS (+ESI): *m*/*z* calcd for $C_{66}H_{55}Au_3P_3$, 1531.251 $[M + H]^+$; found, 1531.249; elemental analysis: calcd for $C_{66}H_{54}Au_3P_3 \cdot \frac{1}{2}H_2O$ (1539.99), C 51.48, H 3.60; found, C 51.45, H 3.66.

C3. (Method B) Prepared from [CTB(H,C_2Au)]$_n$ (0.073 g; 0.0785 × 10^{-3} mol) and PPhMe$_2$ (0.035 mL, 0.034 g; 0.246 × 10^{-3} mol) in a mixture of CH_2Cl_2 (12 mL) and THF (3 mL), 4 h stirring. Yield: 0.081 g (0.0602 × 10^{-3} mol, 77%). Mp 187.5 °C; ^{1}H NMR (500.13 MHz, $CDCl_3$, 295 K): δ (ppm) = 7.724 (m, $^4J_{H,H}$ = 1.5 Hz, $^3J_{H,H}$ = 8.0 Hz, 6 H; *o*- and *o*′-H), 7.480 (d, $^4J_{H,H}$ = 1.5 Hz, 3 H; α′-H), 7.460 (br m, 9 H; *p*-, *m*-, and *m*′-H), 7.244 (d, $^3J_{H,H}$ = 7.5 Hz, 3 H; α-H), 7.177 (dd, $^4J_{H,H}$ = 1.5 Hz, $^3J_{H,H}$ = 7.5 Hz, 3 H; γ-H), 4.743 (d, $^2J_{H,H}$ = 13.5 Hz, 3 H; a-H), 3.624 (d, $^2J_{H,H}$ = 13.5 Hz, 3 H; e-H), 1.747 (d, $^2J_{P,H}$ = 9.5 Hz; CH_3); ^{13}C NMR (125.76 MHz, $CDCl_3$, 295 K): δ (ppm) = 138.83 (s; β′-C), 138.13 (s; β-C), 134.12 (s; α′-C), 132.56 (d, $^1J_{C,P}$ = 56.9 Hz; i-C), 132.16 (d, $^2J_{C,P}$ = 13.8 Hz; *o*- and *o*′-C), 131.75 (s; *p*-C), 130.98 (s; γ-C), 130.22 (s; α-C), 129.29 (d, $^3J_{C,P}$ = 11.6 Hz; *m*- and *m*′-C), 123.47 (s; γ′-C), 104.87, 104.84 (2 s; δ′- and ε′-C), 37.03 (s; CH_2), 15.66 (d, $^1J_{C,P}$ = 35.2 Hz; CH_3); ^{31}P NMR (161.98 MHz, $CDCl_3$, 298 K): δ (ppm) = 14.24 (s); IR (KBr): ν (cm^{-1}) = 3054, 2959 (w), 2920 (s), 2852, 2353, 2331, 2321, 2102, 1750, 1733, 1716, 1696, 1682, 1645 (w), 1600 (m), 1579 (w), 1560 (m), 1543, 1523, 1509 (w), 1487 (s), 1473 (sh), 1457 (w), 1434 (s), 1418 (m), 1396 (w), 1384 (s), 1363, 1340, 1313, 1302, 1108, 1274, 1265, 1237, 1199, 1187, 1161, 1136 (w), 1107 (m), 1095 (sh), 1071 (sh), 1058 (sh), 1047 (sh), 1033 (w), 1022 (w), 1006 (w), 986 (w), 952 (s), 915 (s), 906 (sh), 893 (sh), 840, 805 (m), 739 (s), 718 (m), 688 (s), 633 (m), 612, 590, 572, 561, 548, 536, 521, 513, (w), 483 (s), 461 (w), 446 (sh), 435 (m), 426, 413 (sh); HR-MS (+ESI): *m*/*z* calcd for

$C_{51}H_{49}Au_3P_3$ $[M + H]^+$, 1344.197; found, 1345.202; elemental analysis: calcd for $C_{51}H_{48}Au_3P_3 \cdot \frac{1}{2}H_2O$ (1353.77), C 45.25, H 3.65; found, C 45.23, H 3.74.

C4. (Method A) Prepared from CTB(OMe,C_2H) (0.008 g; 0.0185×10^{-3} mol), [AuCl(PPh_3)] (0.030 g; 0.061×10^{-3} mol), and sodium methoxide (0.025 g; 0.463×10^{-3} mol) in MeOH (5 mL) and THF (5 mL), 4 h stirring. Yield: 0.025 g (0.0138×10^{-3} mol, 75%). (Method B) Prepared from $[CTB(OMe,C_2Au)]_n$ (0.070 g; 0.0686×10^{-3} mol) and PPh_3 (0.058 g; 0.2212×10^{-3} mol) in CH_2Cl_2 (12 mL) and THF (4 mL), 5 h stirring. Yield: 0.082 g (0.0454×10^{-3} mol, 66%). Mp 181 °C; ^{1}H NMR (500.13 MHz, $CDCl_3$, 295 K): δ (ppm) = 7.553 (dd, $^3J_{H,H}$ = 7.8 Hz, $^4J_{H,H}$ = 1.5 Hz, 9 H; *o*-H); 7.528 (dd, $^3J_{H,H}$ = 7.8 Hz, $^4J_{H,H}$ = 1.5 Hz, 9 H; *o*′-H); 7.485 (s, 3 H; α′-H), 7.474 (dd, $^3J_{H,H}$ = 7.8 Hz, $^4J_{H,H}$ = 1.5 Hz, 9 H; *p*-H), 7.429 (dd, $^3J_{H,H}$ = 7.8 Hz, 9 H; *m*-H), 7.425 (dd, $^3J_{H,H}$ = 7.8 Hz, 9 H; *m*′-H), 6.789 (s, 3 H; α-H), 4.679 (d, $^2J_{H,H}$ = 13.5 Hz, 3 H; a-H), 3.898 (s, 9 H; OCH_3), 3.550 (s, $^2J_{H,H}$ = 13.5 Hz, 3 H; e-H); ^{13}C NMR (125.76 MHz, $CDCl_3$, 295 K): δ (ppm) = 159.43 (s; γ-C), 139.92 (s, β-C), 135.83 (s; α′-C), 134.49 (d, $^2J_{C,P}$ = 13.8 Hz; *o*- and *o*′-C), 131.56 (d, $^4J_{C,P}$ = 2.5 Hz; *p*-C), 130.61 (s; β′-C), 130.08 (d, $^1J_{C,P}$ = 55.3 Hz; i-C), 129.18 (d, $^3J_{C,P}$ = 11.3 Hz; *m*- and *m*′-C), 112.67 (s; γ′-C), 111.91 (s; α-C), 99.93, 99.72 (2 s; δ′- and ε′-C), 56.30 (s; OCH_3), 29.83 (s; CH_2); ^{31}P NMR (161.98 MHz, $CDCl_3$, 298 K): δ (ppm) = 42.89; IR (KBr): ν (cm^{-1}) = 3448 (br, m), 3049 (w), 2947 (w), 2843 (w), 2099 (w), 1967 (w), 1892 (w), 1812 (w), 1600 (m), 1493 (s), 1481 (s), 1435 (vs), 1385 (s), 1308 (m), 1265 (s), 1217 (m), 1186 (m), 1142 (m), 1099 (s), 1080 (s), 997 (m), 897 (m), 841 (m), 744 (vs), 711 (m), 692 (vs), 626 (w), 536 (vs), 509 (s); HR-MS (+ESI): *m*/*z* calcd for $C_{84}H_{67}Au_3O_3P_3$, 1807.33; found, 1807.33 $[M + H]^+$; elemental analysis: calcd for $C_{84}H_{66}Au_3O_3P_3 \cdot 3/2CH_2Cl_2$ (1934.66), C 53.08, H 3.60; found, C 52.96, H 3.74.

C5. (Method A) Prepared from CTB(OMe,C_2H) (0.0129 g; 0.0298×10^{-3} mol), [AuCl(PPh_2Me)] (0.040 g; 0.0925×10^{-3} mol), and sodium methoxide (0.032 g; 0.592×10^{-3} mol), overnight stirring. Yield: 0.040 g (0.0247×10^{-3} mol, 83%). (Method B) Prepared from $[CTB(OMe,C_2Au)]_n$ (0.055 g; 0.0539 $\times 10^{-3}$ mol) and PPh_2Me (0.032 mL, 0.0346×10^{-3} g; 0.173×10^{-4} mol) in CH_2Cl_2 (6 mL) and THF (1 mL), 4 h stirring. Yield: 0.074 g (0.0456×10^{-3} mol, 85%). Mp 177.2 °C; ^{1}H NMR (300.13 MHz, $CDCl_3$, 298 K): δ (ppm) = 7.642 (m, $^4J_{H,H}$ = 1.8 Hz, 12 H; *o*- and *o*′-H), 7.468 (s, 3 H; α′-H), 7.451 (d, $^4J_{H,H}$ = 1.8 Hz, 12 H; *m*- and *m*′-H), 7.430 (t, $^4J_{H,H}$ = 1.8 Hz, 6 H; *p*-H), 6.683 (s, 3 H; α-H), 4.679 (d, $^2J_{H,H}$ = 13.5 Hz, 3 H; a-H), 3.888 (s, 9 H; OCH_3), 3.591 (d, $^2J_{H,H}$ = 13.5 Hz, 3 H; e-H), 2.032 (d, $^3J_{H,P}$ = 9.0 Hz, 9 H; CH_3); ^{13}C NMR (125.77 MHz, $CDCl_3$, 295 K): δ (ppm) = 159.44 (s; γ-C), 139.89 (s; β-C), 135.75 (s; α′-C), 132.99 (d, $^2J_{C,P}$ = 13.8 Hz; *o*- and *o*′-C), 131.85 (d, $^1J_{C,P}$ = 55.3 Hz; i-C), 131.52 (s; *p*-C), 130.60 (s; β′-C), 129.21 (d, $^3J_{C,P}$ = 11.3 Hz; *m*- and *m*′-C), 112.72 (s; γ′-C), 111.92 (s; α-C), 100.50 (2 s; δ′- and ε′-C), 55.28 (s; OCH_3), 37.08 (s; CH_2); 14.25 (d, $^1J_{C,P}$ = 34.0 Hz); ^{31}P NMR (161.98 MHz, $CDCl_3$, 298 K): δ (ppm) = 27.15; IR (KBr): ν (cm^{-1}) = 3444 (br, vs), 3074 (sh), 3053 (w), 3022, 3004, 2988, 2959 (sh), 2918, 2849 (m), 2826 (sh), 2353, 2321, 2222, 2104 (w), 1603 (m), 1577, 1561 (w), 1545 (sh), 1494 (m), 1475 (sh), 1458 (d; m), 1435 (s), 1417 (m), 1385 (s), 1333 (w), 1309 (m), 1298 (sh), 1265, 1217, 1182 (m), 1163 (w), 1140, 1103, 1078 (m), 1049, 1029, 1013 (sh), 999 (m), 978, 965 (sh), 948 (w), 893 (s), 857, 841 (m), 813 (sh), 735 (s), 690 (s), 647, 627 (w), 611, 587, 571 (sh), 558 (w), 543 (m), 511 (s), 484, 472, 455, 441, 427, 413 (m); HR-MS (+ESI): *m*/*z* calcd for $C_{69}H_{61}Au_3O_3P_3$ $[M + H]^+$, 1621.283; found, 1621.283; elemental analysis: calcd for $C_{69}H_{60}Au_3O_3P_3 \cdot 2CH_2Cl_2$ (1790.91), C 47.62, H 3.60; found, C 47.66, H 3.62.

C6. (Method A) Prepared from CTB(OMe,C_2H) (0.010 g; 0.0231×10^{-3} mol), AuCl($PPhMe_2$) (0.0944×10^{-3} mol), and NaOMe (0.555×10^{-3} mol) in MeOH (7 mL) and THF (5 mL), 24 h stirring. Yield: 0.018 g (0.0125×10^{-3} mol, 54%). (Method B) Prepared from $[CTB(OMe,C_2Au)]_n$ (0.055 g; 0.054×10^{-3} mol) and $PPhMe_2$ (0.023 g; 0.166×10^{-3} mol) in a mixture of CH_2Cl_2 (12 mL) and THF (3 mL), 5 h stirring. Yield: 0.048 g (0.0335×10^{-3} mol; 62%). Mp 182.5 °C; ^{1}H NMR (400.13 MHz, $CDCl_3$, 298 K): δ (ppm) = 7.738 (m, $^4J_{H,H}$ = 2.0 Hz, 6 H; *o*- and *o*′-H), 7.477 (d, $^4J_{H,H}$ = 2.0 Hz, 9 H; *m*-, *m*′-, and *p*-H), 7.461 (s, 3 H; α′-H), 6.785 (s, 3 H; α-H), 4.681 (d, $^2J_{H,H}$ = 13.6 Hz, 3 H; a-H), 3.889 (s, 9 H; OCH_3), 3.548 (s, $^2J_{H,H}$ = 13.6 Hz, 3 H; e-H), 1.737 (d, $^3J_{H,P}$ = 9.6 Hz, 18 H; CH_3); ^{13}C NMR (125.77 MHz, $CDCl_3$, 295 K): δ (ppm) = 159.47 (s; γ-C), 139.87 (s; β-C), 135.72 (s; α′-C), 132.69 (d, $^1J_{C,P}$ = 54.1 Hz; i-C), 132.19 (d, $^2J_{C,P}$ = 12.6 Hz; *o*- and *o*′-C), 131.70 (s; *p*-C), 130.61 (s, β′-C), 129.25 (d, $^3J_{C,P}$ = 11.3 Hz; *m*- and *m*′-C), 112.79 (s; γ′-C), 111.95 (s; α-C), 100.23 (2 s; δ′- and ε′-C), 56.28 (s; OCH_3), 37.07 (s; CH_2), 15.70 (d; $^1J_{C,P}$ = 35.2 Hz; CH_3); ^{31}P NMR (121.49 MHz, $CDCl_3$, 299 K): δ (ppm) = 14.16; IR (KBr): ν (cm^{-1}) = 3445 (v br, s), 3057, 2961 (w), 2919 (m), 2850 (m), 2360, 2341 (w), 2221 (w), 2100 (w), 1600 (m), 1558 (w), 1491 (s), 1462 (w), 1435 (s), 1422 (w), 1385 (s), 1308 (m), 1263 (s), 1217, 1190, 1147, 1107, 1080 (m), 1042 (w), 1017, 1000, 952 (m), 909 (s), 862 (w), 840 (m), 823, 802, 782 (sh), 742 (s), 722 (m), 691 (s), 645, 623, 608, 583, 561 (w), 542, 515, 488, 447, 430, 408 (m); HR-MS (+ESI): *m*/*z* calcd for $C_{54}H_{55}Au_3O_3P_3$ $[M + H]^+$, 1435.236; found, 1435.236; elemental analysis: calcd for $C_{54}H_{54}Au_3O_3P_3 \cdot \frac{1}{2}C_6H_{12}$ (1476.92), C 46.35, H 4.09; found, C 46.19, H 4.04.

(−)-C2. (Method B) Prepared from $[(-)\text{-}CTB(H,C_2Au)]_n$ (0.010 g; 0.01074×10^{-3} mol) and PPh_2Me (0.0088 mL, 0.0095 g; 0.0474×10^{-4} mol) in a mixture of CH_2Cl_2 (3 mL) and THF (1 mL), 20 min stirring. Yield: 0.013 g (0.0849×10^{-4} mol; 79%).

(+)-C2. (Method B) Prepared from $[(+)\text{-}CTB(H,C_2Au)]_n$ (0.030 g; 0.0322×10^{-3} mol) and PPh_2Me (0.024 mL, 0.0259 g; 1.292×10^{-4} mol) in CH_2Cl_2 (5 mL). Yield: 0.020 g (0.0131×10^{-3} mol; 41%).

(−)-C3. (Method B) Prepared from $[(-)\text{-}CTB(H,C_2Au)]_n$ (0.016 g; 0.0172×10^{-3} mol) and $PPhMe_2$ (0.010 mL, 0.0097 g; 0.0702×10^{-3} mol), in CH_2Cl_2 (2.5 mL). Yield: 0.017 g (0.0126×10^{-3} mol; 73%).

(+)-C3. (Method B) Prepared from $[(+)\text{-}CTB(H,C_2Au)]_n$ (0.040 g; 0.43×10^{-4} mol) and $PPhMe_2$ (25×10^{-3} mL, 0.0243 $\times 10^{-3}$ g; 1.757×10^{-4} mol) in CH_2Cl_2 (6 mL).

(−)-C4. (Method B) Prepared from $[(-)\text{-}CTB(OMe,C_2Au)]_n$ (0.015 g; 0.0147×10^{-3} mol) and PPh_3 (0.0116 g; 0.0442×10^{-3} mol) in CH_2Cl_2 (3 mL) and THF (1 mL). Yield: 0.023 g (0.0127×10^{-3} mol; 86%).

(+)-C4. (Method B) Prepared from $[(+)\text{-CTB(H,C}_2\text{Au})]_n$ (0.016 g; 0.0157×10^{-3} mol) and PPh_3 (0.014 g; 0.0534×10^{-3} mol) in CH_2Cl_2 (4 mL) and THF (2 mL) for 5 h. Yield: 0.016 g (0.00885×10^{-3} mol; 56%).

(−)-C5 and (+)-C5. (Method B) (−)-**C5** was prepared from $[(-)\text{-CTB(OMe,C}_2\text{Au})]_n$ (0.0125 g; 0.0123×10^{-3} mol) and PPh_2Me (0.007 mL, 0.0076 g; 0.038×10^{-3} mol) in CH_2Cl_2 (2.5 mL) and THF (1 mL), overnight stirring. Yield: 0.016 g (0.010×10^{-3} mol; 80%). (Chromatographic separation) Resolution of the **C5** racemate (0.004 g dissolved in 1.2 mL of a mixture of CH_2Cl_2/EtOH/hexane, 50 : 25 : 25) was performed by chiral HPLC using Chiralpak IB column (250 × 4.6 mm), eluting with hexane/EtOH/CH_2Cl_2 40 : 40 : 20 at a flow rate of 1 mL min^{-1} with UV detection at 254 nm. 24 injections of 50 μL each every 10 min were necessary. The first eluted pure enantiomer was (−)-**C5** (1.55 mg) and the second eluted pure enantiomer was (+)-**C5** (1.4 mg).

(−)-C6. (Method B) Prepared from $[(-)\text{-CTB(OMe,C}_2\text{Au})]_n$ (0.0135 g; 0.0132×10^{-3} mol) and $PPhMe_2$ (0.007 mL, 0.0068 g; 0.0492×10^{-3} mol) in CH_2Cl_2 (5 mL) and THF (1 mL). Yield: 0.0133 g (0.00927×10^{-3} mol, 70%); or: resolution of a sample of the racemate prepared according to method A (0.006 g dissolved in 3 mL of a mixture of CH_2Cl_2/hexane, 67 : 33) was performed by chiral HPLC using Chiral Art Cellulose-SJ column (250 × 4.6 mm), eluting with hexane/EtOH/CH_2Cl_2 40 : 20 : 40 at a flow rate of 1 mL min^{-1} and UV detection at 230 nm. 40 injections of 50 μL each every 6.4 min were necessary. The first eluted enantiomer was (+)-**C6** (1 mg) but its optical purity was not satisfactory, and the second eluted enantiomer was pure (−)-**C6** (1.4 mg).

(+)-C6. (Method B) Prepared from $[(+)\text{-CTB(OMe,C}_2\text{PPhMe}_2)]_n$ (0.014 g; 0.0137×10^{-3} mol) and $PPhMe_2$ (0.0071 mL, 0.0069 g; 0.0499×10^{-3} mol) in THF (1 mL) and CH_2Cl_2 (6 mL). Yield: 0.012 g (0.00836×10^{-3} mol; 61%).

Calculation of the structures and of the ECD spectra

Molecular structures of $CTB(H,C_2H)$, $CTB(OMe,C_2H)$, **C1**, **C3** and **C4** were optimized at the DFT level of theory using the Gaussian09 software.[57] The B3LYP functional was used and completed with D3 empirical dispersion correction, together with Def2-TZVPP basis set for light atoms and Def2-TZVPD basis set for Au, including the associated pseudo-potential taken from the Basis Set Exchange library.[58] Frequency calculations were performed in order to check that true energy minima were obtained.

The molecular structures of $CTB(H,C_2H)$, $CTB(OMe,C_2H)$, **C1** and **C4** were also optimized at the DFT level of theory (Gaussian09 software[57]) using the CAM-B3LYP functional together with the 6-311+G(d,p) basis set for light atoms and Def2-TZVPD basis set for Au, including the associated pseudo-potential taken from the Basis Set Exchange library.[58] The solvent effects (CH_2Cl_2) were taken into account through a PCM model. Frequency calculations were performed in order to check that true energy minima were obtained. ECD spectra were calculated by TD-DFT using the same functional and basis sets. The half-widths at half height were adjusted for the comparison of the simulated ECD spectra with the experimental ones.

Author contributions

J. Z. was in charge of the syntheses of the CTBs and their complexes; N. Z. and E. L.-W. carried out the ESI-MS experiments; M. J. and N. V. performed the chiral separations, and recorded the electronic and ECD spectra; E. E. and E. A. were in charge of the DFT calculations. J.-C. C. was responsible for the conceptualization and the methodology of the work, the supervision of J. Z., and the writing of the manuscript.

Conflicts of interest

There are no conflicts to declare.

Acknowledgements

We thank the French National Research Agency (ANR) through the "Programme d'Investissement d'Avenir" under contract 17-EURE-0016 (PhD fellowship to J. Z.), the CNRS, and the University of Strasbourg. Dr Martine Heinrich and Noémie Schneider are thanked for the elemental analyses. E. A. and E. E. are grateful to the EXPLOR mesocenter for providing access to its computing facility (project 2021CPMXX2483).

References

1 Y. Domoto and M. Fujita, *Coord. Chem. Rev.*, 2022, **466**, 214605.
2 M. Yoshizawa, J. K. Klosterman and M. Fujita, *Angew. Chem., Int. Ed.*, 2009, **48**, 3418.
3 T. Murase and M. Fujita, *Chem. Rec.*, 2010, **10**, 342.
4 K. Kobayashi and M. Yamanaka, *Chem. Soc. Rev.*, 2015, **44**, 449.
5 E. G. Percásregui, T. K. Ronson and J. R. Nitschke, *Chem. Rev.*, 2020, **120**, 13480.
6 M. Mastalerz, *Angew. Chem., Int. Ed.*, 2010, **49**, 5042.
7 G. Montà-González, F. Sancenón, R. Martínez-Máñez and V. Martí-Centelles, *Chem. Rev.*, 2022, **122**, 13636.
8 M. Yoshizawa and L. Catti, *Acc. Chem. Res.*, 2019, **52**, 2392.
9 H. Schmidbaur and A. Schier, *Chem. Soc. Rev.*, 2012, **41**, 370.
10 S. S. Batsanov, *Inorg. Mater.*, 2001, **37**, 871.
11 Z. Chen, L. Yang, Y. Hu, D. Wu, J. Yin, G.-A. Yu and S. H. Liu, *RSC Adv.*, 2015, **5**, 93757.
12 V. Cámara, N. Barquero, D. Bautista, J. Gil-Rubio and J. Vicente, *Chem. – Eur. J.*, 2015, **21**, 1992.
13 J. R. Shakirova, M. Shimada, D. A. Olisov, G. L. Starova, H. Nishihara and S. P. Tunik, *Z. Anorg. Allg. Chem.*, 2018, **644**, 308.

14 A. Belyaev, I. Kolesnikov, A. S. Melnikov, V. V. Gurzhiy, S. P. Tunik and I. O. Koshevoy, *New J. Chem.*, 2019, **43**, 13741.
15 M. Głodek, S. Pawlędzio, A. Makal and D. Plażuk, *Chem. – Eur. J.*, 2019, **25**, 13131.
16 W. J. Hunks, M.-A. MacDonald, M. C. Jennings and R. J. Puddephatt, *Organometallics*, 2000, **19**, 6063.
17 V. W.-W. Yam, K.-L. Cheung, S.-K. Yip and K.-K. Cheung, *J. Organomet. Chem.*, 2003, **681**, 196.
18 X. He, E. C.-C. Chen, N. Zhu and V. W.-W. Yam, *Chem. Commun.*, 2009, 4016.
19 L. Rodríguez, M. Ferrer, R. Crehuet, J. Anglada and J. C. Lima, *Inorg. Chem.*, 2012, **51**, 7636.
20 C. P. McArdle, S. Van, M. C. Jennings and R. J. Puddephatt, *J. Am. Chem. Soc.*, 2002, **124**, 3959.
21 A. Schaly, Y. Rousselin, J.-C. Chambron, E. Aubert and E. Espinosa, *Eur. J. Inorg. Chem.*, 2016, 832.
22 A. Schaly, M. Meyer, J.-C. Chambron, M. Jean, N. Vanthuyne, E. Aubert, E. Espinosa, N. Zorn and E. Leize-Wagner, *Eur. J. Inorg. Chem.*, 2019, 2691.
23 Z. Zhong, A. Ikeda, S. Shinkai, S. Sakamoto and K. Yamaguchi, *Org. Lett.*, 2001, **3**, 1085.
24 J. J. Henkelis, C. J. Carruthers, S. E. Chambers, R. Clowes, A. I. Cooper, J. Fisher and M. J. Hardie, *J. Am. Chem. Soc.*, 2014, **136**, 14393.
25 V. E. Pritchard, D. Rota Martir, S. Oldknow, S. Kai, S. Hiraoka, N. J. Cookson, E. Zysman-Colman and M. J. Hardie, *Chem. – Eur. J.*, 2017, **23**, 6290.
26 T. Kojima, F. L. Thorp-Greenwood, M. J. Hardie and S. Hiraoka, *Chem. Sci.*, 2018, **9**, 4104.
27 S. Oldknow, D. Rota Martir, V. E. Pritchard, M. A. Blitz, C. W. G. Fishwick, E. Zysman-Colman and M. J. Hardie, *Chem. Sci.*, 2018, **9**, 8150.
28 E. Britton, R. J. Ansell, M. J. Howard and M. J. Hardie, *Inorg. Chem.*, 2021, **60**, 12912.
29 A. Collet, *Tetrahedron*, 1987, **43**, 5725.
30 A. Collet, J.-P. Dutasta, B. Lozach and J. Canceill, *Top. Curr. Chem.*, 1993, **165**, 103.
31 T. Brotin and J.-P. Dutasta, *Chem. Rev.*, 2009, **109**, 88.
32 G. El-Ayle and K. T. Holman, in *Comprehensive Supramolecular Chemistry II*, ed. J. L. Atwood, 2017, p. 199.
33 T. Brotin, R. Montserret, A. Bouchet, D. Cavagnat, M. Linares and T. Buffeteau, *J. Org. Chem.*, 2012, **77**, 1198.
34 T. Brotin, P. Berthault, D. Pitrat and J.-C. Mulatier, *J. Org. Chem.*, 2020, **85**, 9622.
35 R. M. Fairchild and K. T. Holman, *J. Am. Chem. Soc.*, 2005, **127**, 16364.
36 J. Zhang, A. Schaly, J.-C. Chambron, B. Vincent, N. Zorn, E. Leize-Wagner, M. Jean and N. Vanthuyne, *Chem. – Eur. J.*, 2022, **28**, e202103759.
37 B. M. Schulze, D. L. Watkins, J. Zhang, I. Ghiviriga and R. K. Castellano, *Org. Biomol. Chem.*, 2014, **12**, 7932.
38 L. Peyrard, M.-L. Dumartin, S. Chierici, S. Pinet, G. Jonusauskas, P. Meyrand and I. Gosse, *J. Org. Chem.*, 2012, **77**, 7023.
39 R. J. Cross and M. F. Davidson, *J. Chem. Soc., Dalton Trans.*, 1996, 411.
40 W. Wu, N. Zhu and C.-M. Che, *J. Organomet. Chem.*, 2003, **670**, 11.
41 G. E. Coates and C. J. Parkin, *J. Chem. Soc.*, 1962, 3220.
42 G. Jia, R. J. Puddephatt, J. D. Scott and J. J. Vittal, *Organometallics*, 1993, **12**, 3565.
43 A. Collet and G. Gottarelli, *J. Am. Chem. Soc.*, 1981, **103**, 204.
44 J. Canceill, A. Collet, J. Gabard, G. Gottarelli and G. P. Spada, *J. Am. Chem. Soc.*, 1985, **107**, 1299.
45 A. Collet and G. Gottarelli, *Croat. Chem. Acta*, 1989, **62**, 279.
46 J. Canceill and A. Collet, *New J. Chem.*, 1986, **10**, 17.
47 C. Garcia and A. Collet, *Bull. Soc. Chim. Fr.*, 1995, **132**, 52.
48 J. R. Platt, *J. Chem. Phys.*, 1951, **19**, 263.
49 D. Li, X. Hong, C.-M. Che, W.-C. Lo and S.-M. Peng, *J. Chem. Soc., Dalton Trans.*, 1993, 2929.
50 F. K.-W. Hau, K.-L. Cheung, N. Zhu and V. W.-W. Yam, *Org. Chem. Front.*, 2019, **6**, 1205.
51 H.-S. Lo, N. Zhu, V. K.-M. Au and V. W.-W. Yam, *Polyhedron*, 2014, **83**, 178.
52 T. E. Müller, S. W.-K. Choi, D. M. P. Mingos, D. Murphy, D. J. Williams and V. W.-W. Yam, *J. Organomet. Chem.*, 1994, **484**, 209.
53 Y.-P. Zhou, E.-B. Liu, J. Wang and H.-Y. Chao, *Inorg. Chem.*, 2013, **52**, 8629.
54 Y.-R. Zhenga and P. J. Stang, *J. Am. Chem. Soc.*, 2009, **131**, 3487.
55 Z. Qi, T. Heinrich, S. Moorthy and C. Schalley, *Chem. Soc. Rev.*, 2015, **44**, 515.
56 N. Mézailles, L. Ricard and F. Gagosz, *Org. Lett.*, 2005, **7**, 4133.
57 M. J. Frisch, G. W. Trucks, H. B. Schlegel, G. E. Scuseria, M. A. Robb, J. R. Cheeseman, G. Scalmani, V. Barone, B. Mennucci, G. A. Petersson, H. Nakatsuji, M. Caricato, X. Li, H. P. Hratchian, A. F. Izmaylov, J. Bloino, G. Zheng, J. L. Sonnenberg, M. Hada, M. Ehara, K. Toyota, R. Fukuda, J. Hasegawa, M. Ishida, T. Nakajima, Y. Honda, O. Kitao, H. Nakai, T. Vreven, J. A. Montgomery Jr., J. E. Peralta, F. Ogliaro, M. Bearpark, J. J. Heyd, E. Brothers, K. N. Kudin, V. N. Staroverov, T. Keith, R. Kobayashi, J. Normand, K. Raghavachari, A. Rendell, J. C. Burant, S. S. Iyengar, J. Tomasi, M. Cossi, N. Rega, J. M. Millam, M. Klene, J. E. Knox, J. B. Cross, V. Bakken, C. Adamo, J. Jaramillo, R. Gomperts, R. E. Stratmann, O. Yazyev, A. J. Austin, R. Cammi, C. Pomelli, J. W. Ochterski, R. L. Martin, K. Morokuma, V. G. Zakrzewski, G. A. Voth, P. Salvador, J. J. Dannenberg, S. Dapprich, A. D. Daniels, O. Farkas, J. B. Foresman, J. V. Ortiz, J. Cioslowski and D. J. Fox, *Gaussian 09, Revision D.01*, Gaussian, Inc., Wallingford CT, 2013.
58 B. P. Pritchard, D. Altarawy, B. Didier, T. D. Gibson and T. L. Windus, *J. Chem. Inf. Model.*, 2019, **59**, 4814.